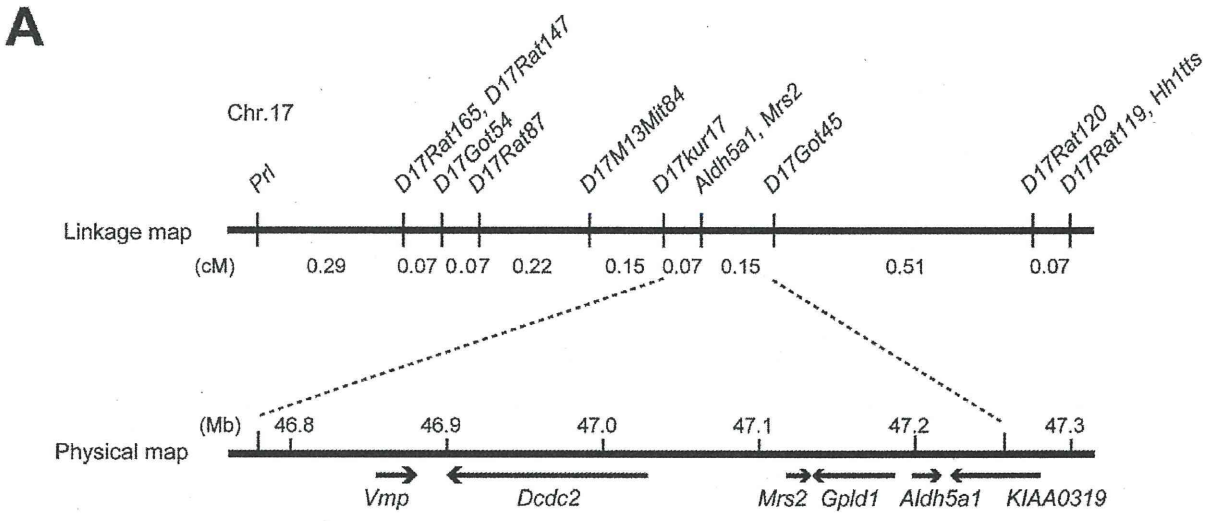
A
Chr.17
Prl
D17Rat165, D17Rat147
D17Got54
D17Rat87
D17M13Mit84
D17kur17
Aldh5a1, Mrs2
D17Got45
D17Rat120
D17Rat119, Hh1tts
Linkage map
(cM)
0.29
0.07
0.07
0.22
0.15
0.07
0.15
0.51
0.07
(Mb)
46.8
46.9
47.0
47.1
47.2
47.3
Physical map
Vmp
Dcdc2
Mrs2
Gpld1
Aldh5a1
KIAA0319

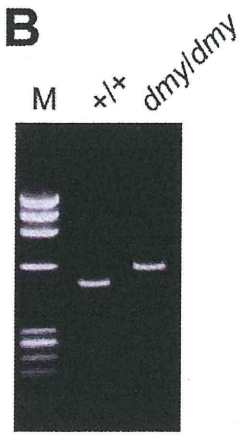
B
M
+/+
dmy/dmy

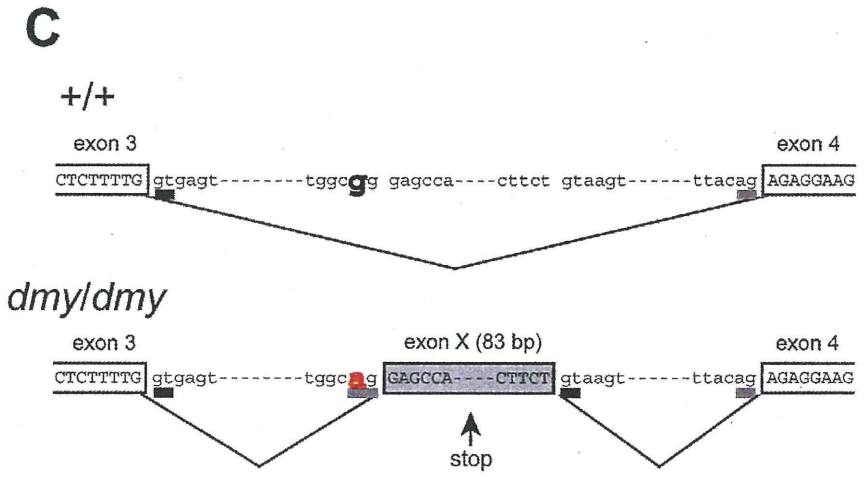
C
+/+
exon 3
exon 4
CTCTTTTG gtgagt--------tggcgg gagcca----cttct gtaagt------ttacag AGAGGAAG
dmy/dmy
exon 3
exon X (83 bp)
exon 4
CTCTTTTG gtgagt--------tggcag GAGCCA----CTTCT gtaagt------ttacag AGAGGAAG
stop

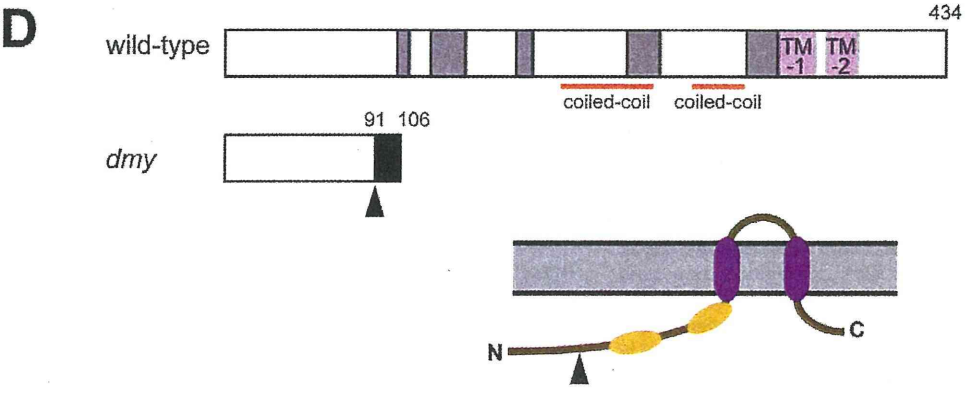
D
wild-type
434
TM -1
TM -2
coiled-coil
coiled-coil
91
106
dmy
N
C

**Figure 2. Positional cloning of the *dmy* mutation.** A. The *dmy* locus was localized within a 0.22-cM region of chromosome 17 between *D17Kur17* and *D17Got45* and no recombination was observed with SSLP markers designed from *Aldh5a1* and *Mrs2* genomic sequences in 1,374 informative meioses. Within the 0.48-Mb physical interval between *D17Kur17* and *D17Got45*, harboring the *dmy* locus, 6 genes: *Vmp* (vesicular membrane protein p24), *Dcdc2* (doublecortin domain containing 2), *Mrs2* (MRS2 magnesium homeostasis factor (*S. cerevisiae*), *Gpld1* (glycosylphosphatidylinositol specific phospholipase D1), *Aldh5a1* (aldehyde dehydrogenase family 5, subfamily A1), and *KIAA0319*, were previously mapped. B. A larger RT-PCR product was obtained when amplifying the 5′ region of *Mrs2* cDNAs from *dmy/dmy* rats with a primer set of rMrs2l-3&4 (5′-TGTACTGATCTACCCGAGTTCC-3′ and 5′-TCTGGAGTTATCACAGCCTTCA-3′). M: molecular marker, ΦX174-*Hae*III digest. C. Upper: Genomic organization in the vicinity of intron 3 of the *Mrs2* wild-type allele. Lower: Genomic rearrangements in the same intron 3 of the $Mrs2^{dmy}$ mutant allele. In the $Mrs2^{dmy}$ mutant allele, a novel splice acceptor site was generated as a consequence of a G-to-A transition at 177 bp downstream of the end of exon 3. An 83-bp genomic sequence (boxed in gray), downstream of the recently generated acceptor site (tggcag), is then inserted into the *Mrs2* mutant transcript. This sequence contains a premature stop codon (vertical arrow), which truncates the protein almost immediately downstream of exon 3. D. Schematic representations of the wild-type and *dmy* MRS2 proteins. Conserved amino acid residues and transmembrane domains are indicated by grey and purple boxes, respectively. Coiled-coil regions are indicated by horizontal orange lines. The position of the *dmy* mutation is indicated by an arrowhead, and the additional 15 residues (GATWTPRILEECLES), indicated by a black box, are deduced to be added subsequently. Bottom: Schematic representation of the topology of MRS2. Purple: transmembrane domains, Orange: coiled-coil regions. The position of the *dmy* mutation is indicated by an arrowhead.
doi:10.1371/journal.pgen.1001262.g002

signals were observed in neurons throughout the CNS. To a lesser extent, astrocytes and oligodendrocytes also exhibited occasional expression of MRS2 (Figure S3). Confocal microscopy demonstrated that MRS2 is located in the mitochondria (Figure 4A–4C). Moreover, immunoelectron microsopic examinations with anti-GFP antibody revealed that MRS2 is localized in the inner membrane of the mitochondria (Figure 4D). MRS2 expression was also observed in the myocardium, liver, testis and skeletal muscles (Figure S4).

### Microglia activation and high expression of inflammatory cytokines were observed in $Mrs2^{dmy}/Mrs2^{dmy}$ rats

Microglial activation, characterized by cellular hypertrophy, has been reported in various dysmyelinating and demyelinating pathologies. To assess microglial activation, we performed immunohistochemistry for IBA1, a specific marker of microglia. In $Mrs2^{dmy}/Mrs2^{dmy}$ rats, prolonged activation of microglia was prominently observed at 6–7 weeks of age (Figure 5A and 5B), the stage at which clinical symptoms such as flaccid paralysis were commonly observed. Expression levels of proinflammatory cytokines, such as *Il1b* and *Il6*, were also significantly higher in $Mrs2^{dmy}/Mrs2^{dmy}$ rats than in wild-type littermates at 6 weeks of age (Figure 5C).

## Discussion

Characterization, by positional cloning, of the molecular defect responsible for the demyelinating phenotype observed in adult *dmy/dmy* rats led us to incriminate a mutation in the *Mrs2* gene. No mutant allele before $Mrs2^{dmy}$, which we report here, has ever been reported at this locus in any mammalian species.

*Mrs2* encodes an inner membrane $Mg^{2+}$ channel in mitochondria and belongs to a family with orthologous copies in a wide range of species [10,12]. *Mrs2* was originally identified in yeast, and orthologous copies of this gene have been identified in a variety of organisms, including bacteria (CorA), fungi (Alr1), and plants (AtMrs2). All proteins in the family have the same substrate selectivity: they transport $Mg^{2+}$, $Co^{2+}$ and some other divalent cations across the mitochondrial membrane. Even if these proteins exhibit relatively low sequence similarities, they all have a few important domains at the same relative position and can functionally complement each other over a wide range of phylogenetic distances [16,17]. In mammals, the normal protein MRS2 has two universally conserved transmembrane domains (TMs) and a conserved Gly-Met-Asn (GMN) motif close to the first TM domain that forms part of the pore and is essential for $Mg^{2+}$ transport [18] (Figure 2D, Figure S5). As we demonstrated, the protein is truncated in *dmy/dmy* mutant rats, having lost both of its essential domains and accordingly its function of an $Mg^{2+}$ transmembrane transporter. In other words, $Mrs2^{dmy}$ is a null allele, which is totally consistent with its recessive allelic interaction.

An MRS2 is a major transport for $Mg^{2+}$ uptake into mitochondria, its function would be expected to be important, if not essential, for the maintenance of respiratory complex I and accordingly for cell viability [6,11]. This assumption was supported by the analysis of MRS2 knock-down, mediated by shRNA in a human HEK-293 cell line, which resulted in a series of physiological changes ranging from transient reduction of $Mg^{2+}$ uptake to the complete loss of mitochondrial respiratory complex I, with decreased mitochondrial membrane potential and cell death, depending on the duration of knock-down treatment [11]. However, if we consider the phenotype of our mutant rat, which is apparently limited to the myelination process with a rather long lifespan, the role of MRS2 in the maintenance of cell integrity should be reconsidered.

Considering the pathological features that appear to be characteristics of the $Mrs2^{dmy}$ allele on the one hand, and MRS2-specific functions, as described above on the other, it is logical to consider that the demyelinating syndrome in mutant rats results from a mitochondrial disease. This assertion is supported by the observation of an elevated rate of lactic acid in the cerebrospinal fluid, reduced ATP in the brain, increased COX activity, and the morphological alteration of mitochondria, which is generally considered a major characteristic of mitochondrial diseases [13–15]. An increase in mitochondria is characteristic of cells with reduced respiratory capacity [19]. The association of mitochondrial dysfunction with demyelination (or leukodystrophy) has been already reported in Leigh syndrome and mitochondrial DNA depletion syndrome [20–23]. The tissues most frequently affected in these mitochondrial diseases are the cerebrum, peripheral nerves, and skeletal muscles, presumably because cells of these tissues require more energy than any other cells in the body. Unfortunately, the detailed pathophysiological mechanism(s) leading to demyelination in these diseases has not yet been unraveled. We consider that our mutant rat could be an interesting tool for investigating this matter.

Mitochondrial dysfunction has also been observed in multiple sclerosis (MS), one of the most common demyelination diseases, but here again many aspects of the pathophysiology require further investigation [24,25]. This difficulty of linking gene functions with a specific syndrome is not so surprising if we consider that, according to the most recent estimates, there may be as many as 1,500 nuclear-encoded mitochondrial proteins [26] and that less than half have been identified with experimental support. Clearly, a complete protein inventory of this organelle

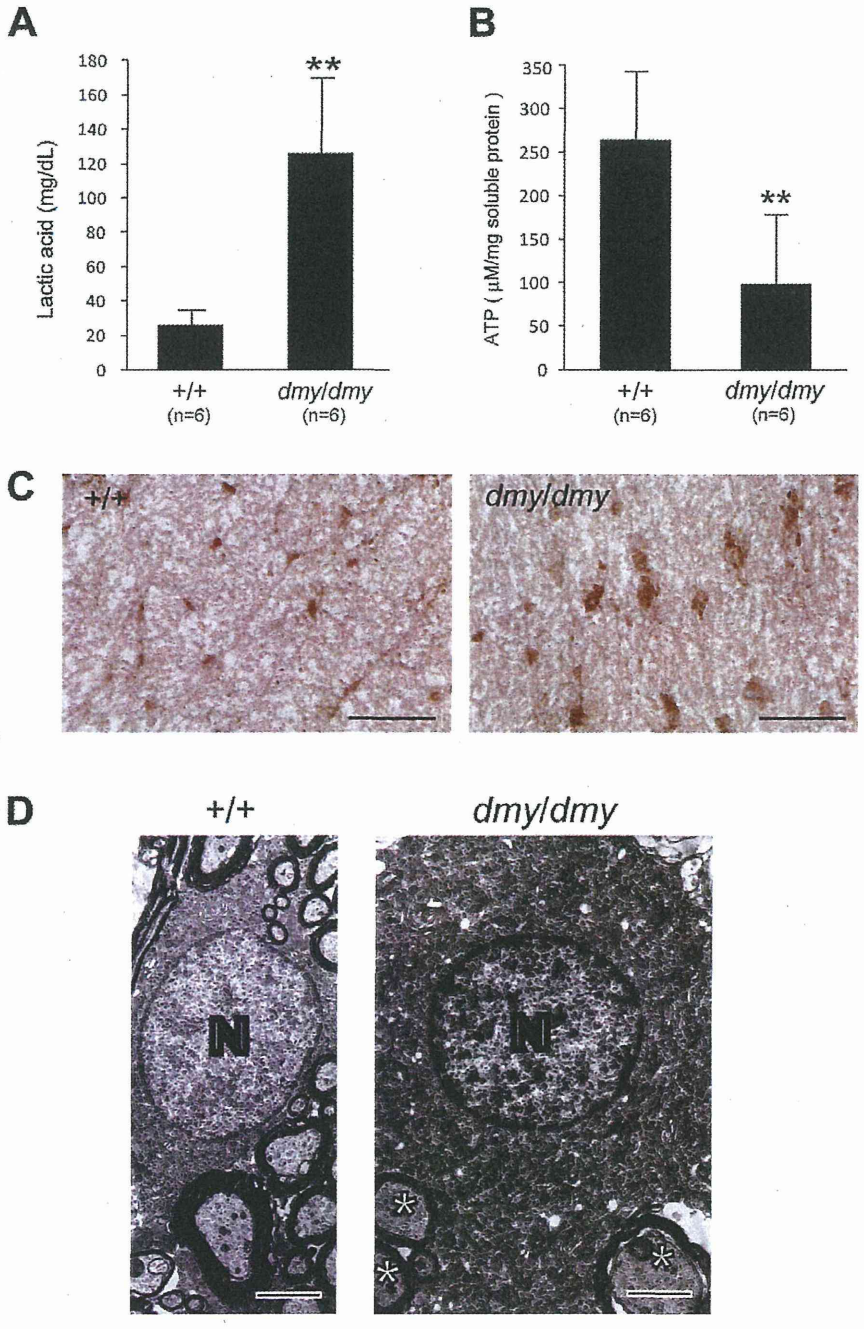


**Figure 3. Biochemical and morphological abnormalities in the mitochondria of *dmy/dmy* mutant rats.** A. Lactic acid concentration in cerebrospinal fluid of 6–7-week-old *dmy/dmy* rats and age-matched wild-type rats. **, P<0.002. B. ATP levels in the brain of 6–7-week-old *dmy/dmy* rats and age-matched wild-type rats. **, P<0.005. C. Cytochrome oxidase staining of the spinal cords of 6–7-week-old *dmy/dmy* (right) and age-matched wild-type (left) rats. Swollen oligodendrocytes were often seen they showed increased COX reaction product. Bar = 50 μm. D. Electron microphotographs of a swollen oligodendrocyte in a *dmy/dmy* rat (right) and an oligodendrocyte in a control wild-type rat. White matter of thoracic spine at 6 weeks of age. N: Nucleus of the oligodendrocyte. Axons adjacent to the oligodendrocyte are indicated by asterisks. Bar = 2 μm.
doi:10.1371/journal.pgen.1001262.g003

across tissues would provide a molecular framework to relate mitochondrial biology and pathogenesis [27].

A point concerning *Mrs2* gene expression in the CNS that is worth noting after our experiments and observations is that the gene in question is expressed at a higher rate in neurons than in oligodendrocytes (Figure 4, Figure S3). This was rather unexpected if we consider that oligodendrocytes are the cells actually responsible for myelination of the CNS. At this time, it remains

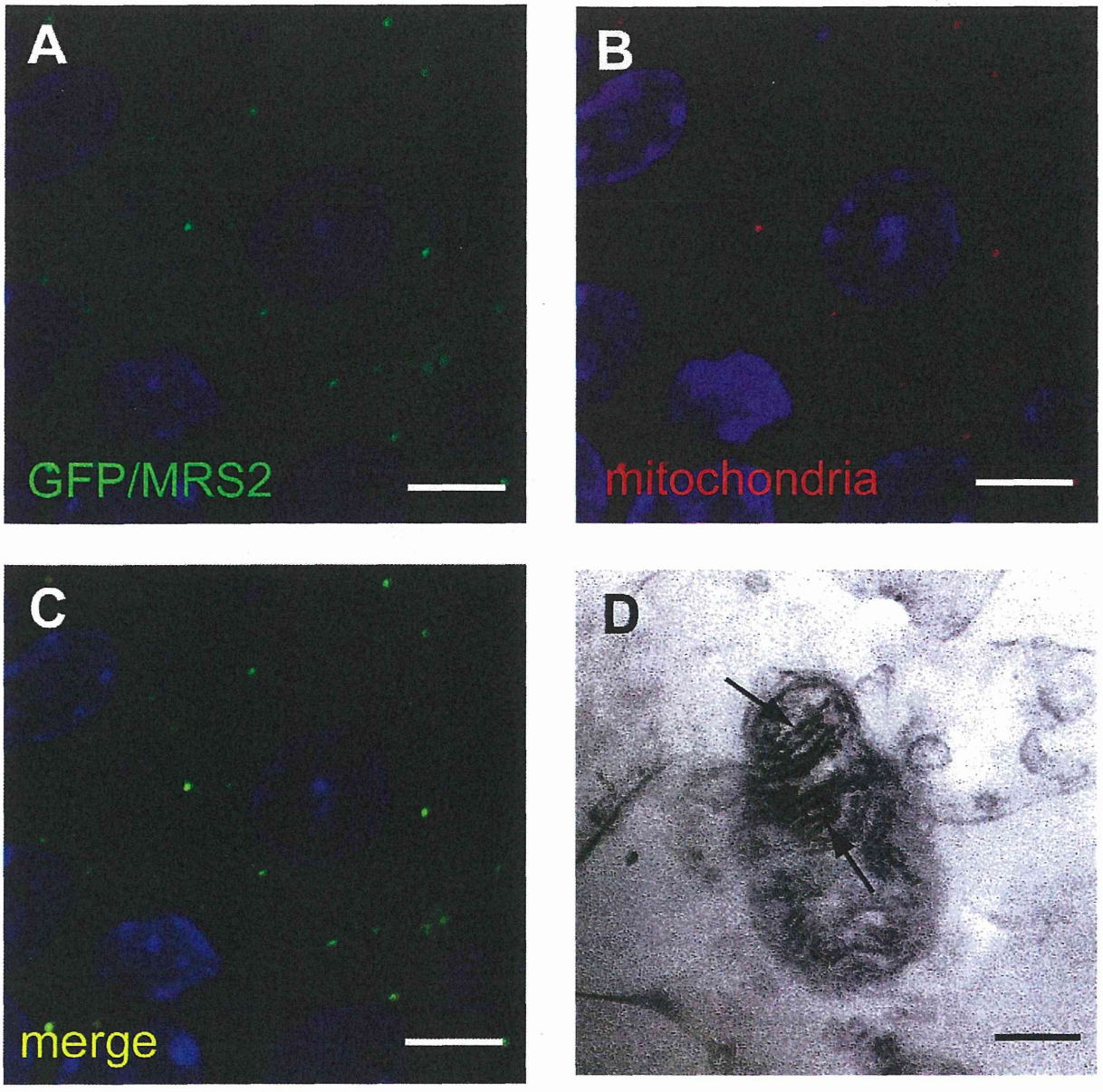


**Figure 4. Expression of MRS2 protein in the mitochondria.** MRS2-GFP recombinant protein (Green) was seen in the cytoplasm of pyramidal cells (A). MRS2-GFP signals were colocalized with the mitochondria (B), as shown in the confocal image of GFP and mitochondrial immunohistochemistry (C). Nuclei were stained with DAPI (Blue). Bar: 5 μm. Immunoelectron microscopy using anti-GFP antibody revealed that MRS2-GFP signals were localized in the inner membrane of the mitochondria (arrows) (D). Bar: 200 nm.
doi:10.1371/journal.pgen.1001262.g004

unclear whether the demyelination in *dmy/dmy* rats is triggered cell-autonomously or cell-nonautonomously. Instead, it is likely that demyelination is enhanced by the surrounding cells, such as activated microglia and astroglia. At 6 weeks of age, when *dmy/dmy* rats began to exhibit ataxia [9], cytokine levels were elevated and microglia were activated (Figure 5), and it is considered that activated microglia cause neuronal damage through the release of potentially cytotoxic molecules, such as proinflammatory cytokines, reactive oxygen intermediates, proteinases, and complement proteins [28]. Oligodendrocytes show greater vulnerability to such molecules [29,30]. Additionally, Kuwamura and co-workers reported prominent astrogliosis and many ED-1-positive macrophages in myelin-destroyed areas [9]. When considered together, these morphological observations led us to believe that the demyelination observed in *dmy/dmy* rats is probably enhanced by activated microglia and astroglia.

In summary, we identified $Mrs2^{dmy}$ as a loss-of-function mutation of the *Mrs2* gene that normally encodes $Mg^{2+}$ transporter protein of the mitochondrial inner membrane. Our observations also demonstrate that the mechanisms underlying the

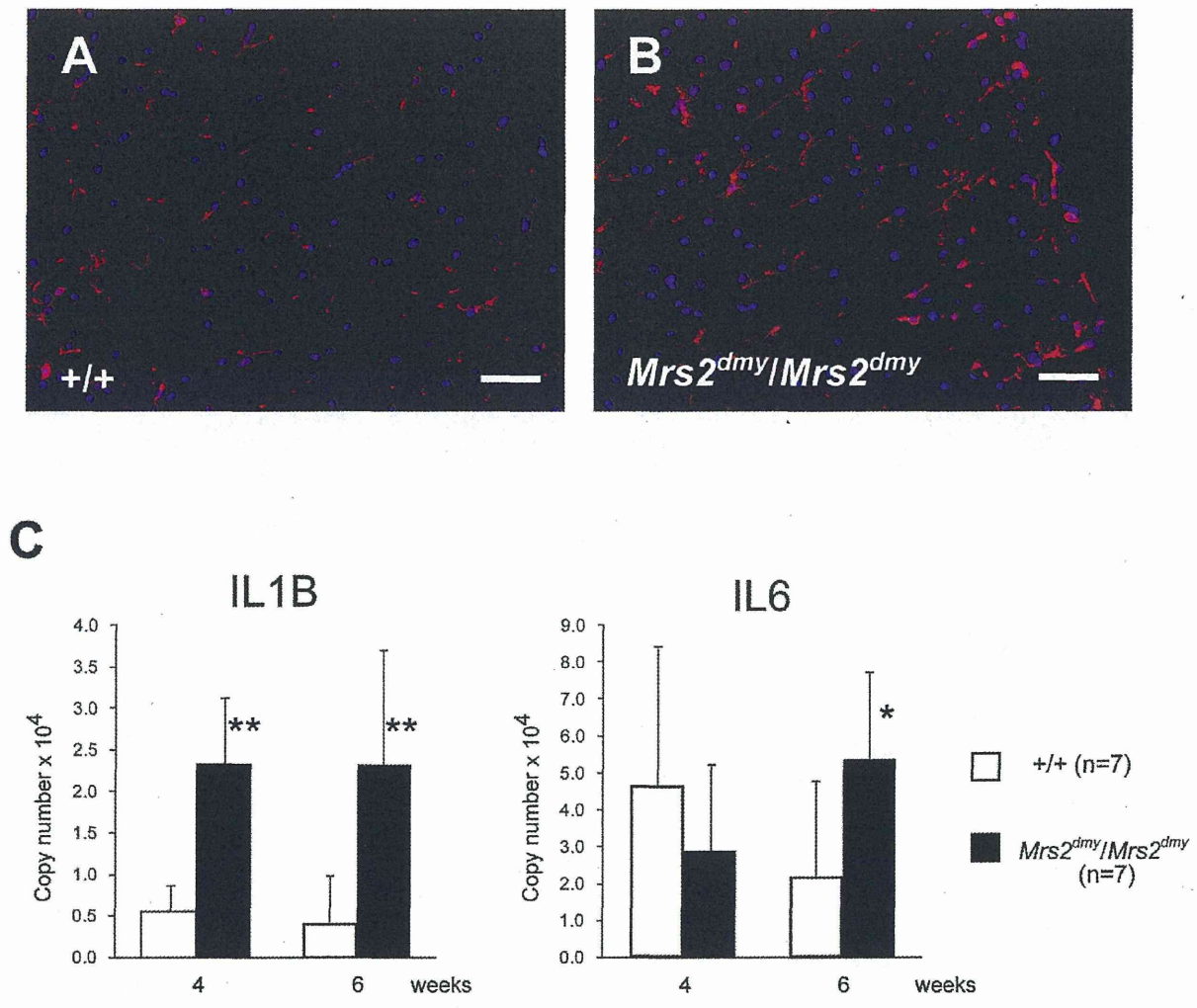


**Figure 5. Activation of microglia in the central nervous system of *Mrs2*$^{dmy}$/*Mrs2*$^{dmy}$ rats.** Immunohistochemistry for Iba1 in the lumbar part of the spinal cord of wild-type (A) and *Mrs2*$^{dmy}$/*Mrs2*$^{dmy}$ rats (B) at 6 weeks of age. Signals of Iba1 (AlexaFluor 546 nm; red), which is upregulated during the activation of microglia, are seen in *Mrs2*$^{dmy}$/*Mrs2*$^{dmy}$ rats much more the wild-type control. Nucleus is stained with DAPI (blue). C, Inflammatory cytokine mRNA expression in the CNS of wild-type (□) and *Mrs2*$^{dmy}$/*Mrs2*$^{dmy}$ (■) rats. IL1b expression was elevated in *Mrs2*$^{dmy}$/*Mrs2*$^{dmy}$ rats at 4 and 6 weeks of age. IL6 was elevated in *Mrs2*$^{dmy}$/*Mrs2*$^{dmy}$ rats at 6 weeks of age. * P<0.05, ** P<0.005.
doi:10.1371/journal.pgen.1001262.g005

initial development of myelin (myelination) are different from those that are involved in its maintenance and turnover since, in *Mrs2*$^{dmy}$/*Mrs2*$^{dmy}$ rats, myelin development is normal while its maintenance is defective. Our mutant rats also appear to be an excellent animal model, not only to evaluate the causal relationships between primary mitochondrial dysfunction and subsequent demyelination, but also for the development of therapies making use, for example, of cell transplantation.

## Materials and Methods

### Genetic fine mapping of *dmy*

Congenic strains WTC (NBRP#0020) and WTC.DMY-*dmy* (NBRP#0021) were both from the National BioResource Project - Rat, Kyoto University (Kyoto, Japan). (WTC.DMY-*dmy* × BN/SsNSlc)F1(+/*dmy*) rats were intercrossed to produce F2 progeny. *dmy*/*dmy* homozygotes were identified at 7–8 weeks of age, when paralysis of the hind limbs was obvious. 687 *dmy*/*dmy* rats were collected out of 3,252 F2 animals (~21%) and used for fine mapping of the *dmy* locus. Simple sequence length polymorphisms (SSLPs) from the *Prl* (prolactin) and *Hh1tts* (Testis-specific histone, H1t and H4t) genes were used for genotyping as described [31]. To refine the limits of the recombinant interval between *Prl* and *Hh1tts*, two gene-specific and one anonymous SSLP markers were used: *Mrs2* (5′-TCTCCCTTGCCTCTATCTCTCGTCT-3′,5′-CCTGCAGTACTGGGTAAGCCTGATG-3′), *Aldh5a1* (5′-GTTAACTGCACAAGAGCAAGCCAGT-3′, 5′-GCTAATGTTAAGTCATGGGGTGAGG-3′), and *D17Kur17* 5′-ACCTCTTTTTGCCAGCATTG-3′, 5′-CCCTGGGATTGGTCCATA-3′).

All animal experiments were approved by the Animal Research Committee of Kyoto University and were conducted according to the Regulations on Animal Experimentation of Kyoto University.

### RT-PCR and direct sequencing

Total RNA was isolated from the brain of 5-week-old animals using ISOGEN (NIPPON GENE, Tokyo, Japan). RT-PCR and direct sequencing of the PCR products were carried out as described previously [32].

### Transgenic rescue and recombinant BAC transgenics

A construct containing the CMV promoter, 1.45-kb of the *Mrs2* coding sequence, and SV40 polyA signal was excised from the vector (pCMV-Script; Agilent Technologies, CA, USA) and used as a transgene, which was microinjected into the pronuclei of fertilized oocytes collected from Crj:Wistar rats. Transgenic offspring founder rats were then crossed with WTC- +/*dmy* rats and then backcrossed again to WTC- +/*dmy* rats to obtain *dmy*/*dmy* homozygous and also hemizygous for the transgene (*dmy*/*dmy*, tg/-). Expression of the transgene was confirmed by RT-PCR with primers (5′-GCGAATGGAGATCCAATTTT-3′, 5′-GGGAGGTGTGGGAGGTTTT-3′) to detect SV40 polyA sequence. Brain RNA was treated with DNase I (New England BioLabs) to remove contaminating genomic DNA and then subjected to cDNA synthesis.

A rat BAC clone, CHORI-230-9K13, including the rat *Mrs2* gene was modified to express MR2SL-EGFP fusion protein under the endogenous promoter by ET recombination technology [33]. Modified genomic DNA was excised from the vector and then used for *in ovo* transgenesis.

### Quantitative PCR

Real-time PCR was performed using the Thermal Cycler Dice Real Time System (Takara Bio Inc., Otsu, Japan) with SYBR Premix Ex Taq II (Takara Bio Inc., Otsu, Japan). By monitoring amplification curves of a test sample and reference samples that contained 101–106 molecules of the gene of interest, the number of target molecules in the test sample was analyzed. The number of target molecules was normalized to that of glyceraldehyde-3-phosphate dehydrogenase (*Gapdh*) as an internal control. The primers used are as follows: 5′-GCTGTGGCAGCTACCTATGTCTTG-3′ and 5′-AGGTCGTCATCATCCCACGAG-3′ for the rat Interleukin-1b (*Il1b*), 5′-CCACTTCACAAGTCGGAGGCTTA-3′ and 5′-GTGCATCATCGCTGTTCATACAATC-3′ for the rat interleukin-6 (*Il6*), 5′-GGCACAGTCAAGGCTGAGAATG-3′ and 5′-ATGGTGGTGAAGACGCCAGTA-3′ for rat *Gapdh*.

### Electron microscopy

Perfusion fixation through the left ventricle was conducted with 4% paraformaldehyde in 0.1 M phosphate buffer (PB). Brains and spinal cords were dissected and stored in 2% paraformaldehyde and 2.5% glutaraldehyde in 0.1 M PB, then post-fixed with 2% osmic acid for 2 hours and embedded in epoxy resin. Ultrathin sections were double-stained with uranyl acetate and lead citrate and examined by a Hitachi H-7500 electron microscope (Hitachi, Tokyo, Japan).

### Immunohistochemistry

Immunohistochemistry was performed as described previously [9]. The following primary antibodies were used: monoclonal anti-2′, 3′-cyclic nucleotide-3′-phosphodiesterase (CNPase) for oligodendrocytes (1:1,000; Sigma, St. Louis, MO, USA), monoclonal anti-mitochondria (1:100; Abcam, Cambridge, MA, USA), polyclonal anti-GFAP for astrocytes (1:1,000; Dako, Carpinteria, CA, USA), polyclonal anti-Iba1 for microglia/macrophages (1:200; Wako Pure Chemical Industries, Osaka, Japan). Cy3-conjugated anti-mouse IgG (1:500; Jackson Laboratories) or Alexa 588-conjugated anti-rabbit IgG (1:500; Molecular Probes) antibody was reacted. Nuclei were counterstained with DAPI (Vactor Laboratories). Signals were detected with a fluorescence microscopy (Olympus, Tokyo, Japan) or a confocal imaging system (C1Si; Nikon, Tokyo, Japan).

For immunoelectron microscopy, PFA-perfused frozen sections were incubated with rabbit antibody against fluorescent protein (1:2,000; Molecular Probes) at 4 °C overnight. After washing in PBS, peroxidase-conjugated anti-rabbit IgG Fab fraction (Jackson Laboratories, 1:1,000) and immunoreactions were reacted 3,3-diaminobenzidine substrate kit (Vector Laboratories), postfixed in 1% osmium tetraoxide, dehydrated in graded ethanol, and then embedded in epoxy resin. Ultrathin sections were examined by electron microscopy (Hitachi, Tokyo, Japan).

### Lactic acid measurements

Cerebrospinal fluid was collected from *dmy*/*dmy*, wild-type littermates, and *dmy*/*dmy* with the normal *Mrs2* transgene at 6–7 weeks of age under isoflurane anesthesia. They were then mixed with 0.8N perchloric acid to inactivate proteins. After centrifugation, lactic acid concentrations of the supernatants were measured by Determiner LA (KYOWA MEDEX Co., Ltd., Tokyo, Japan).

### Cytochrome oxidase histochemistry

Frozen spinal cord sections were prepared. Then, 100 µl of freshly prepared reaction buffer [50 mM Tris/HCl (pH 7.4), 0.5 mg/ml diaminobenzidine, 20 µg/ml catalase and 0.50 mg/ml cytochrome C] was added to each section and slides were incubated for 30 min at 37°C.

### ATP measurements

Rats were sacrificed by cervical dislocation and the brains were immediately excised, frozen in liquid nitrogen, and stored at −80°C until measurement. In order to release cellular ATP, frozen tissue (25 mg) was boiled for 2 min after the addition of 300 µl water containing 100 mM Tris/HCl (pH 7.75) and 4 mM EDTA. Samples were placed on ice and homogenized by sonification (micro tip, 1 s ×10 pulse). ATP concentrations were determined using the ATP bioluminescence assay kit HS II (Roche) according to the manufacturer's protocol. Data were standardized to the protein concentration which was determined by Coomassie Plus – the better Bradford assay kit (Pierce).

### Statistical analysis

Statistical differences in lactic acid, ATP and mRNA expressions between wild-type and *dmy*/*dmy* rats were evaluated using the Mann-Whitney U test.

## Supporting Information

**Figure S1** Detection of the $Mrs2^{dmy}$ mutation. A. Chromatograms showing the $Mrs2^{dmy}$ G-to-A mutation. Upper: wild-type genome. Lower: $Mrs2^{dmy}/Mrs2^{dmy}$ genome. The $Mrs2^{dmy}$ mutation disrupted *Aci*I restriction site (GGCG) in the $Mrs2^{dmy}/Mrs2^{dmy}$ genome. B. Molecular diagnosis of the $Mrs2^{dmy}$ mutation. In the wild type, the 349-bp PCR product amplified with primers rMrs2-31&32 (5′-AAAGTTTGACAAAGAAGGAAACG-3′ and 5′-GGGGATGGAGGGCTATGTAA-3′) is digested with *Aci*I but not in $Mrs2^{dmy}/Mrs2^{dmy}$ mutant rats. M: ΦX174-*Hae*III digests.
Found at: doi:10.1371/journal.pgen.1001262.s001 (1.15 MB TIF)

**Figure S2** Transgenic rescue experiment. A. Expression of the transgene in the brain of a transgenic rat. Brain cDNA from Tg-

positive rats (Lanes 2 and 3) and Tg-negetive rats (Lanes 1and 4) was used as templates. Brain RNA was treated with DNaseI to remove contaminating genomic DNA. M: ΦX174 *Hae*III digests. B. Histopathology of the cervical part of the spinal cord of *dmy/dmy* transgene-negative rats (left) and *dmy/dmy* transgene-positive (right) rats aged 10 weeks. Luxol fast blue-HE staining. Original magnification: ×100. C. Lactic acid concentration in cerebrospinal fluid of 6-7-week-old *dmy/dmy* rats and age-matched *dmy/dmy Mrs2* cDNA-transgenic rats. Elevated lactic acid (126 ± 43.7 mg/dL) was reduced to normal level (22 ± 3.1 mg/dL). **, $P < 0.002$. D. Electron microphotograph of an oligodendrocyte in a *dmy/dmy* transgene-positive rat. Densely packed mitochondria (arrowheads) were found in the cytoplasm. Bar: 2μm.
Found at: doi:10.1371/journal.pgen.1001262.s002 (5.52 MB TIF)

**Figure S3** MRS2 expression in the CNS of Mrs2-GFP recombinant BAC transgenic rats. MRS2 signals were mainly found in neurons (A), and occasionally in GFAP-positive astrocytes (B) and CNP-positive oligodendrocytes (C). Left: Bar: 50 μm. Center, Right: Bar: 20 μm.
Found at: doi:10.1371/journal.pgen.1001262.s003 (3.15 MB TIF)

**Figure S4** MRS2 expression in Mrs2-GFP recombinant BAC transgenic rats. MRS2 signals were observed in the myocardium (A), liver (B), testis (C) and skeletal muscles (D). Bar: 50 μm.
Found at: doi:10.1371/journal.pgen.1001262.s004 (6.29 MB TIF)

**Figure S5** Sequence alignment of yeast, human, and rat MRS2 proteins. Predicted transmembrane domains (TM-1, TM-2) are boxed; * indicates identical residues; : indicates conservative substitution; . indicates semiconservative substitutions. The sequence of a motif conserved in all putative magnesium transporters, G-M-N, is indicated in bold. Predicted coiled-coil regions are underlined, five regions with conserved amino acid residues (CRB-1-5; conserved residue block) are shaded grey. Arrowhead: The position of the residue affected by the *dmy* mutation, after which the 15 additional residues follow in mutant MRS2.
Found at: doi:10.1371/journal.pgen.1001262.s005 (1.38 MB TIF)

## Acknowledgments

The authors are grateful to M. Yokoe for excellent technical assistance.

## Author Contributions

Conceived and designed the experiments: TK. Performed the experiments: TK MK ST TI YN KK. Analyzed the data: TK MK. Contributed reagents/materials/analysis tools: MA TS. Wrote the paper: TK MK JLG.

## References


1. Werner H, Jung M, Klugmann M, Sereda M, Griffiths IR, et al. (1998) Mouse models of myelin diseases. Brain Pathol 8: 771–793.
2. Griffiths IR (1996) Myelin mutants: model systems for the study of normal and abnormal myelination. Bioessays 18: 789–797.
3. Meyer Zu Horste G, Nave KA (2006) Animal models of inherited neuropathies. Curr Opin Neurol 19: 464–473.
4. Kuramoto T, Sotelo C, Yokoi N, Serikawa T, Gonalons Sintes E, et al. (1996) A rat mutation producing demyelination (*dmy*) maps to chromosome 17. Mamm Genome 7: 890–894.
5. Kitada K, Guenet JL, Serikawa T (2000) Determination of the mouse homologous region for the rat *dmy* locus. J Exp Anim Sci 41: 40–43.
6. Schindl R, Weghuber J, Romanin C, Schweyen RJ (2007) Mrs2p forms a high conductance $Mg^{2+}$ selective channel in mitochondria. Biophys J 93: 3872–3883.
7. Gregan J, Bui DM, Pillich R, Fink M, Zsurka G, et al. (2001) The mitochondrial inner membrane protein Lpe10p, a homologue of Mrs2p, is essential for magnesium homeostasis and group II intron splicing in yeast. Mol Gen Genet 264: 773–781.
8. Schock I, Gregan J, Steinhauser S, Schweyen R, Brennicke A, et al. (2000) A member of a novel Arabidopsis thaliana gene family of candidate $Mg^{2+}$ ion transporters complements a yeast mitochondrial group II intron-splicing mutant. Plant J 24: 489–501.
9. Kuwamura M, Kanehara T, Tokuda S, Kumagai D, Yamate J, et al. (2004) Immunohistochemical and morphometrical studies on myelin breakdown in the demyelination (*dmy*) mutant rat. Brain Res 1022: 110–116.
10. Kolisek M, Zsurka G, Samaj J, Weghuber J, Schweyen RJ, et al. (2003) Mrs2p is an essential component of the major electrophoretic $Mg^{2+}$ influx system in mitochondria. Embo J 22: 1235–1244.
11. Piskacek M, Zotova L, Zsurka G, Schweyen RJ (2009) Conditional knockdown of hMRS2 results in loss of mitochondrial $Mg^{2+}$ uptake and cell death. J Cell Mol Med 13: 693–700.
12. Wiesenberger G, Waldherr M, Schweyen RJ (1992) The nuclear gene MRS2 is essential for the excision of group II introns from yeast mitochondrial transcripts in vivo. J Biol Chem 267: 6963–6969.
13. Devivo DC (1993) The expanding clinical spectrum of mitochondrial diseases. Brain Dev 15: 1–22.
14. Huttemann M, Zhang Z, Mullins C, Bessert D, Lee I, et al. (2009) Different proteolipid protein mutants exhibit unique metabolic defects. ASN Neuro 1.
15. Thambisetty M, Newman NJ (2004) Diagnosis and management of MELAS. Expert Rev Mol Diagn 4: 631–644.
16. Bui DM, Gregan J, Jarosch E, Ragnini A, Schweyen RJ (1999) The bacterial magnesium transporter CorA can functionally substitute for its putative homologue Mrs2p in the yeast inner mitochondrial membrane. J Biol Chem 274: 20438–20443.
17. Zsurka G, Gregan J, Schweyen RJ (2001) The human mitochondrial Mrs2 protein functionally substitutes for its yeast homologue, a candidate magnesium transporter. Genomics 72: 158–168.
18. Eshaghi S, Niegowski D, Kohl A, Martinez Molina D, Lesley SA, et al. (2006) Crystal structure of a divalent metal ion transporter CorA at 2.9 angstrom resolution. Science 313: 354–357.
19. Detmer SA, Chan DC (2007) Functions and dysfunctions of mitochondrial dynamics. Nat Rev Mol Cell Biol 8: 870–879.
20. Hung PC, Wang HS (2007) A previously undescribed leukodystrophy in Leigh syndrome associated with T9176C mutation of the mitochondrial ATPase 6 gene. Dev Med Child Neurol 49: 65–67.
21. Navarro-Sastre A, Martin-Hernandez E, Campos Y, Quintana E, Medina E, et al. (2008) Lethal hepatopathy and leukodystrophy caused by a novel mutation in MPV17 gene: description of an alternative MPV17 spliced form. Mol Genet Metab 94: 234–239.
22. Spinazzola A, Viscomi C, Fernandez-Vizarra E, Carrara F, D'Adamo P, et al. (2006) MPV17 encodes an inner mitochondrial membrane protein and is mutated in infantile hepatic mitochondrial DNA depletion. Nat Genet 38: 570–575.
23. Zafeiriou DI, Koletzko B, Mueller-Felber W, Paetzke I, Kueffer G, et al. (1995) Deficiency in complex IV (cytochrome c oxidase) of the respiratory chain, presenting as a leukodystrophy in two siblings with Leigh syndrome. Brain Dev 17: 117–121.
24. Andrews HE, Nichols PP, Bates D, Turnbull DM (2005) Mitochondrial dysfunction plays a key role in progressive axonal loss in Multiple Sclerosis. Med Hypotheses 64: 669–677.
25. Mahad DJ, Ziabreva I, Campbell G, Lax N, White K, et al. (2009) Mitochondrial changes within axons in multiple sclerosis. Brain 132: 1161–1174.
26. Lopez MF, Kristal BS, Chernokalskaya E, Lazarev A, Shestopalov AI, et al. (2000) High-throughput profiling of the mitochondrial proteome using affinity fractionation and automation. Electrophoresis 21: 3427–3440.
27. Pagliarini DJ, Calvo SE, Chang B, Sheth SA, Vafai SB, et al. (2008) A mitochondrial protein compendium elucidates complex I disease biology. Cell 134: 112–123.
28. Dheen ST, Kaur C, Ling EA (2007) Microglial activation and its implications in the brain diseases. Curr Med Chem 14: 1189–1197.
29. Merrill JE, Scolding NJ (1999) Mechanisms of damage to myelin and oligodendrocytes and their relevance to disease. Neuropathol Appl Neurobiol 25: 435–458.
30. Mitrovic B, Ignarro LJ, Montestruque S, Smoll A, Merrill JE (1994) Nitric oxide as a potential pathological mechanism in demyelination: Its differential effects on primary glial cells in vitro. Neuroscience 61: 575–585.
31. Serikawa T, Kuramoto T, Hilbert P, Mori M, Yamada J, et al. (1992) Rat gene mapping using PCR-analyzed microsatellites. Genetics 131: 701–721.
32. Kuramoto T, Kitada K, Inui T, Sasaki Y, Ito K, et al. (2001) Attractin/mahogany/zitter plays a critical role in myelination of the central nervous system. Proc Natl Acad Sci U S A 98: 559–564.
33. Zhang Y, Buchholz F, Muyrers JP, Stewart AF (1998) A new logic for DNA engineering using recombination in *Escherichia coli*. Nat Genet 20: 123–128.

*Exp. Anim. 60(1), 57–63, 2011*

—Original—

# Kyoto Rhino Rats Derived by ENU Mutagenesis Undergo Congenital Hair Loss and Exhibit Focal Glomerulosclerosis

Takashi KURAMOTO[1)], Mitsuru KUWAMURA[2)], Fumi TAGAMI[1)], Tomoji MASHIMO[1)], Masato NOSE[3)], and Tadao SERIKAWA[1)]

*[1)]Institute of Laboratory Animals, Graduate School of Medicine, Kyoto University, Sakyo-ku, Kyoto 606-8501, [2)]Laboratory of Veterinary Pathology, Osaka Prefecture University, Izumisano, Osaka 598-8531, and [3)]Department of Pathogenomics, Graduate School of Medicine, Ehime University, Toon, Ehime 791-0295, Japan*

**Abstract:** *N*-ethyl-*N*-nitrosourea (ENU) mutagenesis is an important tool for studying gene function and establishing human disease models. Here, we report the characterization of a novel hairless mutant rat strain that carries a recessive mutation called Kyoto rhino (*krh*), which was created by ENU-mutagenesis. We produced a F344-*krh* strain through inbreeding without backcrossing to F344 rats. The *krh*/*krh* rats lost their coat hair by eight weeks of age. They also developed wrinkled skin, cystic hair canals and long curved nails by four months of age. Markedly dilated hair follicles that contained keratin debris were observed during histological analysis of the skin. The *krh* locus was mapped near the hairless (*Hr*) gene on chromosome 15. Sequence analysis revealed a nonsense mutation (c. 1238 C>A, p. S413X) in the *Hr* gene. The truncated HR protein was deduced to lack a zinc-finger domain and repression domains. In aged $Hr^{krh}/Hr^{krh}$ rats, focal glomerulosclerosis (FGS) was observed in which collapsed glomeruli contained protein exudates in Bowman's capsule. Mesangial matrices that had proliferated in segments and foot processes that were fused in podocytes were also observed. The $Hr^{krh}/Hr^{krh}$ rats also suffered from significant proteinuria. Given its breeding history, the F344-$Hr^{krh}$ strain may harbor ENU-induced mutation(s) that underlie FGS in addition to having the $Hr^{krh}$ mutation. The F344-$Hr^{krh}$ rat is a useful model of skin disease and may provide a new model system for the examination of the pathogenesis of FGS.

**Key words:** disease model, hairless, mutation, nephrosis

## Introduction

Hairless mutant rodents are valuable models for studying molecular mechanisms that underlie hair growth control. They are particularly valuable when searching for the genetic basis of hereditary human hair disorders.

In mice, 43 mutations are responsible for primary genetic hairlessness [7]. Among them, the most important are allelic mutations of the hairless (*Hr*) gene. The best characterized allele is the hairless (*hr*). $Hr^{hr}/Hr^{hr}$ mice have a striking total alopecia phenotype which appears between three and four weeks of age. The pheno-

*(Received 17 August 2010 / Accepted 16 September 2010)*

*Address corresponding: T. Kuramoto, Institute of Laboratory Animals, Graduate School of Medicine, Kyoto University, Yoshidakonoe-cho, Sakyo-ku, Kyoto 606-8501, Japan*

type originates in the periorbital region and propagates in a wave-like fashion in the rostral-to-caudal direction [20]. It has been determined, through comparative studies of several distinct mouse *Hr* mutations, that the *Hr* gene product plays a key role in controlling hair follicle transformation during the catagen phase [20]. The hairless phenotype of *Hr*-mutant mice ($Hr^{hr}/Hr^{hr}$) is similar to that of the human disease atrichia. The disease phenotype comprises papular lesions (APL) and alopecia universalis congenital (ALUNC), complete hair loss after birth. It is a result of human *HR* mutation [2, 4, 9].

Another important mutant *Hr* of the mouse is the rhino (*rh*) mouse. $Hr^{rh}/Hr^{rh}$ mice lose all of their hair by seven weeks of age, possess wrinkled skin and their nails overgrow. Additionally, they develop an autoimmune disease characterized by hypergammaglobulinemia, immunoglobulin deposits in the basement membrane of skin, spleen, liver, and kidney, and the presence of antinuclear antibodies which appear in young mice and increase with age [14].

Several rat hair loss mutations have been described. They are for the Charles River hairless rat [1], the Iffa Credo (IC) rat [6], the Hairless Wistar Yagi rat also known as the HWY/Slc rat [13], the Dundee experimental bald rat also known as the DEBR rat [22], the Bald rat [12], and the Hirosaki hairless rat (HHR) [17]. An intragenic deletion in the desmoglein 4 gene underlies the IC rat skin phenotype [6]. The absence of 80-kb of genomic DNA that contains five basic keratin genes is the cause of the HHR rat hairless phenotype [17].

Rat hair follicles are larger than those of mice. Therefore hairless mutant rats are attractive models for studying hair follicle development, differentiation, and cycling. Rat mutants are also good models for evaluating the effects of new drugs for treating human skin diseases. Therefore, it would be beneficial to establish new hairless rat models for these purposes.

We recently treated rats with *N*-ethyl-*N*-nitrosourea (ENU) to obtain different mutants [16]. Several hair loss phenotypes were identified by employing phenotype-driven screening. A hair loss mutant line was established by crossing mutant-type males with wild-type female littermates. Our analysis of the breeding record of this line can be used to prove that the hair loss phenotype is autosomal recessive. Thus, the mutation was named Kyoto rhino (*krh*).

In this study, we identified the *krh* mutation using a positional candidate approach and characterized the *krh*/*krh* rats. *krh* is a nonsense mutation of the rat *Hr* gene. *krh*/*krh* rats develop renal failure with massive proteinuria and focal glomerulosclerosis (FGS).

## Materials and Methods

*Animals*

ENU-treated F344/NSlc male rats were mated with F344/NSlc female rats to generate $G_1$ offspring [16]. The ENU-mutagenized $G_1$ rats (n=42) were used as founders for the phenotype-driven screening of recessive mutations. Briefly, the $G_1$ rats were crossed with two F344 rats to generate $G_2$ offspring. The female $G_2$ offspring were then backcrossed with their parental $G_1$ rats to generate $G_3$ offspring. The recessive mutations induced by ENU in the $G_1$ rats become homozygous in the $G_3$ rats. Among the $G_3$ offspring (n=11) from a $G_1$ male (#E2307), three rats showed a hair loss phenotype; these rats were probands (P generation). We mated the affected rats with the normal littermates to fix the hair loss phenotype. The phenotype was fixed at the $F_2$ generation and the mutation was called *krh*. A mutant line was established by employing brother-sister mating (homozygous male × heterozygous female). The generation of inbreeding had reached $F_6$ at the end of August, 2010. The animal care and experimental procedures that were used were approved by the Animal Research Committee, Kyoto University and were carried out according to the Regulation on Animal Experimentation at Kyoto University.

*Genetic mapping*

Twenty $N_2$ rats were produced from a (BN/SsNSlc × F344-*krh*/*krh*)$F_1$ × F344-*krh*/*krh* backcross. The genotypes for the *krh* locus were identified on the basis of coat phenotype at four to five weeks of age. Genomic DNA was prepared from tail biopsies using an automatic DNA purification system (PI-200, Kurabo, Japan) and genotypes for *D15Rat10*, *D15Rat13*, and *D15Rat85* were determined. Linkage relationship was evaluated using the chi-square test of the Excel statistical package.

Confidence intervals ($P<0.05$) were calculated according to the method of a previous report [11].

*RT-PCR and direct sequencing*

Total RNA was isolated from the skin of five-week-old animals using ISOGEN (NIPPON GENE, Tokyo, Japan). RT-PCR and direct sequencing of the PCR product was carried out as described previously [15]. Rat *Hr* cDNA was amplified using the following eight primer sets: rHr-01&02 CACCTGTGGAAGGCTGCT and ACAGGGTCACTCTTGGGATG; rHr-03&04 AGGGACTACGCTGGAAGGAA and CCCAAACGTTACCGAGAGTG; rHr-05&06 GCAGGCAGCAGAATCTTTG and TCCTGTGGATGTCTCTGGTG; rHr-07&08 ACTCAAGAGGGCAGGCAGT and GGTGTTGAAGAGTCCGTGGT; rHr-09&10 CTTCCATCAACAAGGGCCTA and CTGGGCTCTCTGTGGAGTCT; rHr-11&12 GGTCAGCAGAAGGAACCAAC and TTCCAGAATGCTGTGCTGTC; rHr-13&14 GACTTAGCCTGTGGGGAATG and CTCCAAGGTTCCTGCTCCAG; rHr-15&16 GTCTCCAGGTAGCCAGACCA and GTTCCCTGCTTGTACCCAAA. The PCR products overlapped each other and spanned the entire 3,624 bp *Hr* coding sequence (CDS).

*Morphological analysis*

Dorsal and ventral skin samples were collected from *krh/krh* and *krh/+* littermates at two, nine and seventeen weeks of age. Mouse anti-cytokeratin (AE1/AE3, Dako Japan, Tokyo, Japan) was used for immunohistochemical analysis of the skin samples. Bound antibody was detected using horseradish peroxidase conjugated anti-mouse antibody (Histofine Simplestain MAX-PO; Nichirei, Tokyo, Japan) and 3,3'-diaminobenzidine as a chromogen (Vector Laboratories, Burlingame, CA, USA). To detect lipids, frozen sections were made from specimens that had been fixed with formalin and they were stained with Oil red O.

Organ samples of the heart, lungs, liver, pancreas, kidneys, spleen, lymph nodes, salivary glands, lacrimal glands, thyroid gland, adrenal glands, small and large intestines, and knee and foot joints, were collected from three *krh/krh* rats and three F344 rats at 40 weeks of age. They were fixed using 10% neutral buffered formalin, embedded in paraffin, cut at 4 $\mu$m in thickness, and then stained with hematoxylin and eosin (HE). To study glomerular lesions, periodic acid-Schiff (PAS) or periodic acid-methenamine-silver (PAM) staining was employed. For immunofluorescence studies, kidney samples were frozen in 22-oxacalcitriol compound (Miles Inc., Elkhart, IN, USA).

*Electron microscopy*

Perfusion fixation through the left ventricle was conducted with 4% paraformaldehyde in 0.1 M phosphate buffer (PB). Kidneys that had been excised were stored in 2% paraformaldehyde and 2.5% glutaraldehyde in 0.1 M PB. They were fixed with 2% osmic acid for 2 h and embedded in epoxy resin. Ultra-thin sections were double-stained with uranyl acetate and lead citrate and examined using a Hitachi H-7500 electron microscope (Hitachi, Tokyo, Japan).

*Urine protein measurement*

To collect urine, six male *krh/krh* rats and six F344/NSlc (+/+) rats, 40 weeks of age, were caged individually in metabolic chambers after they had been orally loaded with physiological saline at 2.5 ml/100 g body weight. Six-hour urine samples were collected and their volumes, and protein concentrations were determined. Statistical differences were determined using the Mann-Whitney U test.

## Results

*krh/krh rat hair loss phenotype and skin morphology*

For the *krh/krh* rats, hair loss first occurred around the nose around 2 weeks after birth and extended gradually from the anterior to the posterior of the body (Fig. 1A and 1B). At around four months of age they had wrinkled skin, cystic hair canals and long curved nails.

Through histopathological analysis, markedly dilated hair follicles were observed. These cystic follicles contained a lot of keratin debris (Fig. 1C), and they stained positive for cytokeratin (Fig. 1D). The cysts were lined by a thin layer of squamous epithelium and an easily identifiable granular cell layer. The sebaceous glands that surrounded the dilated cysts were hyperplastic. Staining with Oil red O revealed that a large amount of lipids was present in the lumen of each cyst and on the